Journal of Wind Engineering & Industrial Aerodynamics 207 (2020) 104394

Contents lists available at ScienceDirect

Journal of Wind Engineering & Industrial Aerodynamics

journal homepage: www.elsevier.com/locate/jweia

Time-cost "trade-off" analysis for wind-induced inhabitability of tall buildings equipped with tuned mass dampers

Wei Cui [a,b,c,*], Teng Ma [b], Luca Caracoglia [d]

[a] State Key Lab of Disaster Reduction in Civil Engineering, Tongji University, Shanghai, 200092, China
[b] Department of Bridge Engineering, College of Civil Engineering, Tongji University, Shanghai, 200092, China
[c] Key Laboratory of Transport Industry of Bridge Wind Resistance Technologies, Tongji University, Shanghai, 200092, China
[d] Department of Civil & Environmental Engineering, Northeastern University, Boston, MA, 02115, USA

ARTICLE INFO

Keywords:
Tall buildings
Wind-induced vibration
Tuned mass damper
Occupants' comfort
Loss of functionality
Downtime

ABSTRACT

One of the major concerns for tall buildings is the extreme accelerations induced by wind loads and perceived by their occupants. Normally, tuned-mass dampers (TMD) are installed on tall buildings to suppress vibration. However, an established procedure to evaluate the impact of the TMD system from the standpoint of financial profit/deficit is not readily available. This study proposes a framework that integrates local wind climate, wind-induced vibration and TMD performance analysis in terms of monetary outcomes. The proposed framework is composed of three parts: 1) evaluation of wind speed probability distribution at the building site; 2) calculation of wind-induced structural acceleration and its mitigation by TMD with variable mass ratio; 3) lifetime "net profit" assessment, based on the annual normalized inhabitable floor area. A feasibility study suggests that, for super-tall buildings, the TMD is financially effective in reducing wind-induced vibration and inhabitable floor area. Furthermore, large TMD is unnecessary and can lead to a financial deficit. Finally, a simulated mid-rise building does not require a TMD since the financial benefit is marginal.

1. Introduction

In several metropolitan cities around the world, skyscrapers are regional landmarks, such as the Central Park Tower in New York, Burj Khalifa in Dubai, and The Shard in London. They have a large impact on human and social activities. They have greatly reshaped local society from the perspectives of culture and economy. Meanwhile, they are located close to coastal areas and are threatened by high wind loads. Therefore, it is required to evaluate building safety and serviceability under extreme wind hazards. In the recent decade, performance-based design (PBD) has been emerging as an innovative and alternative design tool as opposed to the traditional load-resistance principles, which are normally prescribed in design codes. PBD was initially developed for structural seismic engineering, the purpose of which is ensuring the structural performance objectives for several recurrence intervals associated with various natural or man-made hazard intensities (SEAOC, 1995; Inokuma, 2002). The implementation of PBD is to design structures to satisfy a set of prescribed performance requirements against various hazards, including earthquake, wind, and blast loads (Barbato et al., 2014).

In the wind engineering field, a series of studies inspired by PBD from seismic engineering have been recently implemented (Ciampoli et al., 2011). Initially, Performance-based wind engineering (PBWE) was applied to low-rise residential buildings (Ellingwood et al., 2004; van de Lindt and Dao, 2009), where structural collapses are normally triggered by failure of weak key members, such as beam-column joints.

In recent years, because of increasing residents' comfort requirements, excessive vibrations causing discomfort to occupants has become a major challenge of structural design for slender, tall buildings. Researchers around the world (Kwok et al., 2009; Bernardini et al., 2012, 2013) have proposed several wind-induced vibration and performance evaluation methods, along with several optimization algorithms emphasizing residents' comfort (Spence and Kareem, 2014; Bernardini et al., 2013). Recent studies have advanced PBWE for other types of dynamic sensitive structures, such as pedestrian bridges (Rizzo et al., 2018), long-span bridges (Seo and Caracoglia, 2012, 2013) and tall buildings (Cui and Caracoglia, 2018b). A recent study (Cui and Caracoglia, 2020) has been devoted to the numerical calculation and wind climate parametric analysis of intervention costs induced by repeated,

* Corresponding author. 207 Wind Engineering Building, Tongji University, 1239 Siping Road, Shanghai, 200092, China.
E-mail addresses: cuiwei@tongji.edu.cn (W. Cui), tjtmmt@tongji.edu.cn (T. Ma), lucac@coe.neu.edu (L. Caracoglia).

https://doi.org/10.1016/j.jweia.2020.104394
Received 9 March 2020; Received in revised form 20 September 2020; Accepted 20 September 2020
Available online 1 October 2020
0167-6105/© 2020 Elsevier Ltd. All rights reserved.

catastrophic wind events during building lifetime. The research has been inspired by similar research on structural performance and monetary loss investigation in earthquake engineering (Wen and Kang, 2001). Related research has been expanded through academic collaboration among research groups (Ierimonti et al., 2016, 2017). Finally, the PBWE theory for vertical structures has been considerably revised to include thunderstorm downburst loads (Le and Caracoglia, 2018) and tornadic loads (Le and Caracoglia, 2020).

Despite these advancements, Cui and Caracoglia (2020) provide a novel perspective to consider the influence of multiple, moderate, or mild wind events, which may frequently happen during structural lifetime. Moderate or mild wind hazards may not damage structural elements. However, they can interrupt residential activities and cause business downtime to either a portion or the whole structure. Consequently, indirect financial losses due to downtime, in the context of cost-benefit analysis, should be considered as an integral part of a life-cycle performance analysis.

For super-tall buildings, installation of a tuned mass damper (TMD) is considered to suppress wind-induced vibration and improve structural performance (Kwok and Samali, 1995; Elias and Matsagar, 2017, 2018). Recent studies also demonstrate that distributed, multiple TMDs are effective to suppress wind-induced vibration (Elias et al., 2019b, a; Pozos-Estrada, 2018) of slender structures. The same approach may be employed to control seismic-induced vibration (Pozos-Estrada and Gómez, 2019).

Pozos-Estrada et al. (2011) and Pozzuoli et al. (2013) investigated the Reliability and cost-effectiveness of installing TMD on tall buildings to reduce wind-induced vibrations. Ierimonti et al. (2018) analyzed the benefits of installing a TMD in terms of life-cycle cost savings due to a reduction of wind-induced damage. Nevertheless, besides the initial installation cost, the TMD itself will occupy building (floor) space, whose financial profit will be permanently lost.

Therefore, the decision of TMD installation cannot exclusively consider vibration suppression but also examine the ''opportunity cost'', i.e. the indirect cost that includes, apart from the TMD installation, any floor space losses. This *modus operandi* refers to the ''internalization'' of external costs, i.e. an implementation of cost-benefit analysis that is routinely employed in finance and economics to justify long-term investments but is quite uncommon in the field of wind engineering. The ''trade-off'' between positive financial income derived from reducing the inhabitable building floor areas during wind events and negative opportunity cost emerging from both TMD installation cost and permanently reduced floor space, occupied by TMD, should be carefully balanced by the wind engineers.

Capitalizing on the recent developments in financial engineering, this study will provide a rigorous, analytically-based and numerically-implemented approach to quantify the trade-off costs vs. benefits. This approach provides a conceptual and feasibility framework to evaluate monetary benefits associated with TMD installation in a tall building, which can assist designers and stakeholders examine the financial plan during initial design.

2. Theoretical background

2.1. Parent wind speed probability distribution

The prediction of wind hazard intensity (wind speed), such as typhoons, monsoons, etc. is an interdisciplinary field between engineering and meteorology. Since these extreme weather phenomena threaten the structural safety and building functional integrity, quantifying the probability distributions of the wind hazards is always the first step of the PBWE analysis.

Hourly records of wind speeds are usually extracted from a historical database, recorded by a meteorological station located in the proximity of the proposed project site (Simiu and Yeo, 2019). The advantage of a parent wind speed probability distribution is that all weather records, including wind speed and direction, are standardized and reliable; weather stations (NOAA, 2015) are usually present everywhere, especially in the USA. However, the recording history at most weather stations is relatively short compared to the typical structural design life (between 50 and 100 years). Therefore, parent wind records must be appropriately extrapolated to a longer time duration (50 or 100 years). In the case of mixed wind climates, tropical cyclone wind speeds must be accounted for; normally, these are synthetically generated either by numerical methods (Vickery et al., 2000) or physical models (Emanuel et al., 2006).

However, parent probability distribution of mean wind speeds is widely used for building serviceability evaluation, such as pedestrian wind micro-climate analysis (Lawson, 1978) for built environment exposed to periodically repeated moderate-speed wind events. Normally, the parent wind speed probability distribution can be approximately modeled using a Weibull model (Cui and Caracoglia, 2020). If wind directionality is considered, the joint probability density function (PDF) of the correlated mean-wind speed and direction can be simulated by linear-angular model, as described by Carta et al. (2008).

2.2. Frequency domain response analysis

For a tall building against wind effects, whose main concern is usually the serviceability limit states, an elastic dynamic model with linearized turbulence effects is adequate (Davenport, 1988). The standard random vibration theory, transformed in the frequency domain, is widely used.

The study by (Cui and Caracoglia, 2018a) provides a set of analytical formulations for the coupled multi-mode and multi-directional wind--induced response in matrix format. For mode j, the generalized scalar dynamic equation in the dimensionless frequency domain is:

$$\frac{8m_{0,j}\pi^2}{\rho D^4 h}\left[f^2+2\xi_{0,j}f_{0,j}\iota f-f_{0,j}^2\right]\widehat{\chi}_j(f)+\sum_{k=1}^{N}\left[s_{j,k}+\iota f c_{j,k}\right]\widehat{\chi}_k(f)=q_j \tag{1}$$

In Eq. (1), $m_{0,j}$ is the generalized modal mass, which is calculated as $m_{0,j}=\int_0^\infty \varphi_j(z)^2 m(z)\mathrm{d}z$ with $\varphi_j(z)$ being a generic, dimensionless, continuous mode shape function and $m(z)$ the mass per unit height; D and h are the reference building dimensions respectively, $f=nD/U_h$ is the normalized frequency, $f_{0,j}$ is the j-th normalized structural modal frequency, $\xi_{0,j}$ is the structural damping ratio of the j-th mode, $s_{j,k}$ and $c_{j,k}$ are the elements of the aeroelastic stiffness and damping matrices with N modes being considered, q_j is the generalized modal wind force in the frequency domain and $\widehat{\chi}_j$ is the generalized modal displacement in the frequency domain with $\iota=\sqrt{-1}$. The off-diagonal elements of the aeroelastic stiffness and damping matrices, $s_{j,k}$ and $c_{j,k}$ ($j\neq k$), account for inter-modal coupling and are influenced by fluid-structure interaction effects (Denoël, 2009).

2.3. Structural vibration suppression with TMD

With the help of a TMD system, the wind-induced vibration can be mitigated (Kwok and Samali, 1995). In the frequency domain, the structural vibration can be derived using power spectral density (PSD) function, in a scalar form, as:

$$S_{\chi_j\chi_j}(f)=\left|H_j(f)\right|^2 S_{q_jq_j}(f) \tag{2}$$

where $S_{\chi_j\chi_j}(f)$ is the PSD of structural vibration in generalized coordinates χ_j, and $S_{q_jq_j}(f)$ is the generalized wind force in the corresponding coordinate. $H_j(f)$ is the transfer function, simultaneously accounting for the structural dynamic behavior and TMD control system. The function $H_j(f)$ can be expressed as (Xu et al., 1992):

$$\left|H_j(f)\right|^2 = \frac{\left(\gamma^2-\lambda^2\right)^2 + 4\gamma^2\lambda^2\xi_j^2}{\left(2\pi n_{0,j}\right)^4 m_{0,j}^2\left(a^2+b^2\right)} \tag{3a}$$

$$a = \lambda^4 - \lambda^2\left(1+\gamma^2+\mu\gamma^2+4\xi_{0,j}\xi_j\gamma\right)+\gamma^2 \tag{3b}$$

$$b = 2\lambda\left[\xi_j\gamma\left(1+\lambda^2-\mu\lambda^2\right)+\xi_{0,j}\left(\gamma^2-\lambda^2\right)\right] \tag{3c}$$

where μ is TMD mass ratio $\mu = m/m_{0,j}$ (with m TMD mass and $m_{0,j}$ modal mass, defined earlier), $f_{0,j}$ is the normalized structural modal frequency without TMD, f_j is the normalized TMD reference frequency, $\gamma = n_j/n_{0,j} = f_j/f_{0,j}$ is the TMD frequency ratio, $\lambda = n/n_{0,j} = f/f_{0,j}$ is the reference frequency ratio, ξ_j is the damping ratio of TMD system for mode $j\{=x, y\}$, a and b are calculation coefficients.

When the damper mass m is 0 (without TMD), the transfer function becomes:

$$\left|H_{0,j}(f)\right|^2 = \frac{1}{\left(1-\lambda^2\right)^2 + 4\xi_{0,j}^2\lambda^2} \tag{4}$$

For the evaluation of structural performance against wind hazards, the maximum or RMS resultant response, i.e. displacement and acceleration, should be the modulus combining the two or three horizontal motion components, orthogonal along-wind, and cross-wind directions, and the torsionally-induced lateral deflections. Because the resultant displacement does not follow the Gaussian process assumption, translation process theory (Grigoriu, 1984) is used to calculate the equivalent maximum resultant response.

2.4. Proposed life-cycle downtime estimation

The life-cycle cost analysis, originally developed for building damage caused by earthquakes (Wen and Kang, 2001), has been adapted to PBWE. The life-cycle analysis is able to compute the total lifetime cost of a structure including initial construction, intervention cost, repair cost, and maintenances cost from a probabilistic perspective.

Besides life-cycle cost, Cui and Caracoglia (2020) suggest that out-of-service downtime caused by wind-induced vibration, rarely included in the financial loss analysis, should be considered besides the intervention cost analysis associated with physical damage and repair.

Moderate or mild wind-induced interruptions often happening frequently (more than once each year), and the corresponding downtime due to temporary floor space inhabitability, caused by vibration, can be calculated through the portion of exceeded wind speeds over the parent wind speeds distribution.

The life-cycle cost estimation formula can be adjusted to include the out-of-service downtime calculation equation in Eq. (5):

$$T = 8766\int_0^{2\pi}\int_0^{\infty} r(\theta,U_h) f_{\mathrm{p}}(\theta,U_h)\mathrm{d}v\mathrm{d}\theta \tag{5}$$

In the previous equation $T(t)$ is out-of-service inhabitable time in term of hours for year t; $f_{\mathrm{p}}(\theta,U_h)$ is the distribution of the parent, hourly-averaged wind speed and the associated mean-wind direction θ; $r(\theta,U_h)$ is the ratio of the out-of-service space area with respect to the total building floor area at various wind speeds U_h and directions θ; 8766 is the average total hours in one year. The reference wind speed U_h is evaluated at the building roof height $z = h$ (Cui and Caracoglia, 2020). Eq. (5) can be reduced to obtain the normalized downtime, which is the ratio between expected annual out-of-service time and the total hours of one year (8766), as

$$\Gamma = \int_0^{2\pi}\int_0^{\infty} r(\theta,U_h) f_{\mathrm{p}}(\theta,U_h)\mathrm{d}v\mathrm{d}\theta \tag{6}$$

Unlike wind-induced damage, inhabitable downtime for certain floor area during a moderate-speed wind event may happen frequently; however, the affected areas can usually resume to normal operating conditions immediately after the event. Inhabitable area ratio $r(\theta,U_h)$, which is a new quantity proposed in Cui and Caracoglia (2020), is employed in Eq. (6) to describe the dependence of the habitability on the different wind event intensities.

RMS acceleration is employed in this study as the main serviceability limit indicator, since it is normally associated with motion sickness due to wind-induced vibration (Pozos-Estrada et al., 2010). For a specific tall building, RMS accelerations at roof-top $\sigma_a(h)$ and at a middle-level floor $\sigma_a(h/2)$ can be computed using the frequency domain analysis formulas in Section 2.3 with and without TMD. For a standard shear-type building, the two primary sway mode shape functions are linear along the height and, therefore, the RMS value of accelerations increases linearly as well with building elevation. The lowest elevation z_s (Kwok et al., 2009) within which a given threshold s is exceeded, can be derived through linear interpolation or extrapolation between rooftop and middle level accelerations. Consequently, the inhabitable area ratio $r(\theta,U_h)$ becomes

$$r(\theta,U_h) = \frac{h-z_s}{h} = \left.\frac{\sigma_a(h)-s}{2[\sigma_a(h)-\sigma_a(h/2)]}\right|_{\theta,U_h} \tag{7}$$

where s is the RMS acceleration threshold, which is assumed as 1.42 gal $\left[\mathrm{cm}\cdot\mathrm{s}^{-2}\right]$ corresponding to residential building requirement (Isyumov, 1993). Since mode shape functions are assumed as linear along z in each primary direction (i.e. a shear-type building), the inhabitable area ratio based on the definition of $r(\theta,U_h)$ can be suitably used as the tall building performance indicator against wind; resorting to more complex performance evaluation functions, as for example defined in Yang et al. (2004), is not necessary.

In this initial conceptual study, directionality is not considered. Omni-directional, uniform wind direction assumption is employed; thus Eq. (6) is reduced to

$$\Gamma = \int_0^{\infty} r(U_h) f_{\mathrm{p}}(U_h)\mathrm{d}U_h \tag{8}$$

3. Cost trade-off analysis method for tall buildings equipped with TMD

As stated in the previous section, large wind-induced vibration will cause partial building functionality loss, which will indirectly reduce the expected business profit. Installation of a TMD usually suppresses wind-induced vibration and enhances residential comfort in a tall building (Ierimonti et al., 2018; Giaralis and Petrini, 2017; Petrini et al., 2020). However, besides the initial installation cost, the TMD itself occupies the building's upper floors, which is normally a highly profitable space. Thus, it is necessary to balance the benefit and cost of TMD installation.

Combining benefit and cost, the lifetime net profit consequent to a TMD installation is:

$$C(t) = \int_0^t (\Gamma_0-\Gamma)A_f p\exp(-\delta\tau)\mathrm{d}\tau - C_i - \int_0^t A_d p\exp(-\delta\tau)\mathrm{d}\tau \tag{9}$$

In the above equation, C_i is the initial construction cost of certain TMD, p is the annual commercial profit of unit floor area; A_f and A_d respectively are whole building floor area and area occupied by the TMD system; Γ and Γ_0 respectively are annual, cumulative relative downtime

area [Eq. (8)] with and without TMD; $\exp(-\delta\tau)$ expresses the financial time effect (Wen and Kang, 2001) and δ is the annual discount rate. The rate δ is normally assumed to be 5%. The above equation can be further simplified to:

$$C(t) = p\left[(\Gamma_0 - \Gamma)A_f - A_d\right]\frac{1-\exp(-\delta t)}{\delta} - C_i \tag{10}$$

The most important factor for TMD design is the mass ratio μ. Generally, a larger μ yields enhanced vibration suppression. However, a larger μ requires a larger floor space and more expensive installation cost. Therefore, for a specific tall building, the cost vs. benefit also depends on μ:

$$C(t;\mu) = p\left[(\Gamma_0 - \Gamma(\mu))A_f - A_d(\mu)\right]\frac{1-\exp(-\delta t)}{\delta} - C_i(\mu) \tag{11}$$

Without any loss of generality, the cost $C(t;\mu)$ can be normalized by unit area profit p. The previous equation can be further simplified as:

$$c(t;\mu) = \left[(\Gamma_0 - \Gamma(\mu))A_f - A_d(\mu)\right]\frac{1-\exp(-\delta t)}{\delta} - c_i(\mu) \tag{12}$$

where $c(t;\mu) = C(t;\mu)/p$ and $c_i(\mu) = C_i(\mu)/p$.

The procedure for evaluating Eq. (12) above is schematically illustrated in Fig. 1.

4. Numerical examples

4.1. Benchmark building structure: CAARC

Detailed description of the benchmark building structure can be found in Appendix A.

Because there are unavoidable wind-tunnel errors in the building model setup and force measurements, uncertainties related to several key aerodynamic coefficients (Cui and Caracoglia, 2020) should be considered in the simulation of the wind-induced vibration. In a similar way, the randomness in the structural properties must also be included. The probability distributions of the considered random parameters are listed in Table 1. The statistics of the structural parameters is derived from Spence and Kareem (2014), and aerodynamic parameters from Cui and Caracoglia (2020). Monte Carlo simulation with sample size equal to 5000 is performed to analyze the parameter uncertainty effect; averaged structural responses are used to evaluate the building performance.

Similarly, wind-induced accelerations combining both along-wind and cross-wind horizontal, directional components and the corresponding inhabitable area ratio can be calculated. Fig. 2 illustrates roof-top RMS accelerations from 100 samples of the Monte Carlo simulations and the averaged values from 5000 samples; the corresponding inhabitable area ratios are also plotted with the RMS acceleration threshold. Meanwhile, the roof-top RMS accelerations $\tilde{\sigma}_a(h)$ without considering the structural and aerodynamic parameters are also plotted in Fig. 2 as the reference value to demonstrate the uncertainty effect. It can be found out that the mean value of $\sigma_a(h)$ from Monte Carlo simulation marginally increased compared with $\tilde{\sigma}_a(h)$, and the randomness originating from the structural and aerodynamic parameters will increase the expected wind-induced vibration of the benchmark tall building.

Subsequently, wind-induced vibration at various reference wind speeds and corresponding inhabitable area ratios, for the CAARC building equipped with TMD, can be calculated for each implementation of Monte Carlo simulations. The averaged results are plotted in Fig. 3. Initially, a TMD with $\mu = 0.2\%$ was selected since it is very effective for vibration suppression and reduction of inhabitable area ratio Γ. Fig. 4 plots the inhabitable area ratio r and rooftop accelerations $\sigma_a(h)$ for the CAARC building equipped with TMD with $\mu = 0.2\%$. By comparing with Fig. 2, the TMD is effective to reduce both the accelerations and inhabitable ratio. Similar to the tall building without TMD, the parameter randomness will slightly increase the expected wind-induced vibrations.

However, the marginal benefit of increasing the TMD mass decreases rapidly. Thus, it is necessary to find the optimal TMD mass. This operation can be performed using several, equivalent approaches; one of these approaches is presented in Appendix B.

Table 1
Statistics of the uncertain structural and aerodynamic parameters.

Variables	Mean	Coefficient of variation	Type of distribution
Drag Coefficient C_D	1.4	0.0357	Gamma
Derivative of lift coefficient, $\partial C_L/\partial\theta$	−3.5	0.0143	Normal
Standard deviation of lift coefficient, C_{Ls}	0.1435	0.1394	Gamma
Fundamental natural frequencies, $n_{0,x}$, $n_{0,y}$	0.2	0.3	Lognormal
Structural damping ratios, $\xi_{0,x}$, $\xi_{0,y}$	0.01	0.01	Lognormal

4.2. Wind climate

Integrated Surface Database at meteorological Station 583211 is employed as the source of hourly wind speed data records. This station is located along the runway at the Shanghai Pudong International Airport in Shanghai, China, and its anemometer is installed at 10 m above ground. Normally, the exposure category close to an airport can be roughly considered as open terrain $z_0 = 0.02$ m, and then can be converted to other exposure categories (Irwin, 2006). The power law is used to describe the boundary-layer wind speed profile from $z = 10$ m to the reference building height (rooftop) $h = 183$ m. According to ASCE-7 16 (ASCE, 2016), this is equal to $U(z) = U_{10}(z/10)^{0.28}$ for category B exposure.

The histogram of the parent wind speed and the distribution fitted by the Weibull model are plotted in Fig. 5.

4.3. Lifetime cost-benefit analysis for the CAARC building

By integrating the building inhabitable area ratio $r(U_{10})$, referenced to U_{10} in Fig. 3 with the wind speed probability distribution $f_p(U_{10})$ in Fig. 5, the normalized annual inhabitable area ratio for the CAARC building without TMD Γ_0 and with TMD $\Gamma(\mu)$ can be calculated using Eq. (8) and shown in Fig. 6. Similar to Fig. 3, a TMD with low mass ratio μ can effectively reduce structural vibration and downtime. Nevertheless, the effectiveness rapidly diminishes as μ increases.

Before completing the cost-benefit analysis, additional assumptions are needed to describe the financial parameters and building configurations.

First, the whole building floor area is:

$$A_f = B \times D \times \left\lfloor \frac{h}{d_f} \right\rfloor \tag{13}$$

where $\lfloor . \rfloor$ is the integer floor indicator-operator and d_f is the average inter-story height, which is assumed as 4 m.

Next, the area occupied by the TMD is assumed proportional to the damper mass:

$$A_d(\mu) = \Lambda \times \mu \times m_{0,j} = \Lambda \times \mu \times \int_0^h M\varphi(z)_j \mathrm{d}z \tag{14}$$

where Λ is the mass to area conversion factor, which is assumed as 0.0004.

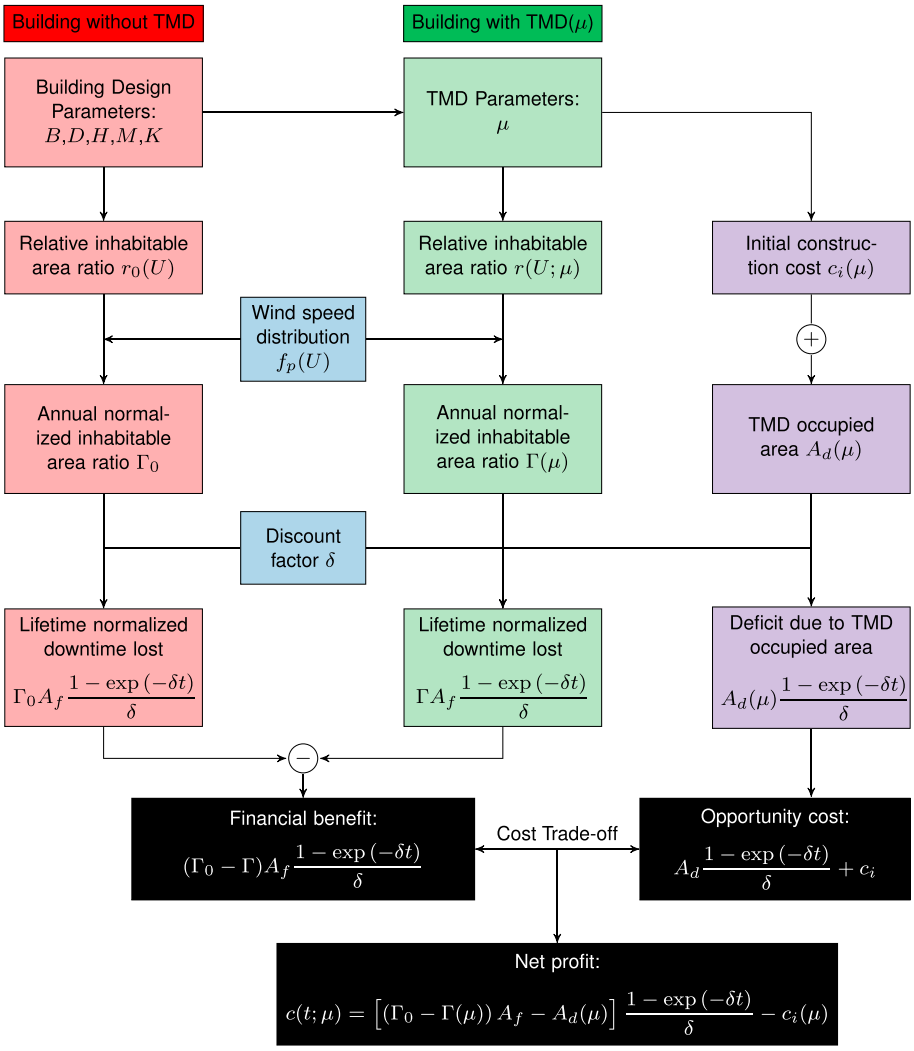

Fig. 1. Flow chart for tall building TMD cost trade-off analysis.

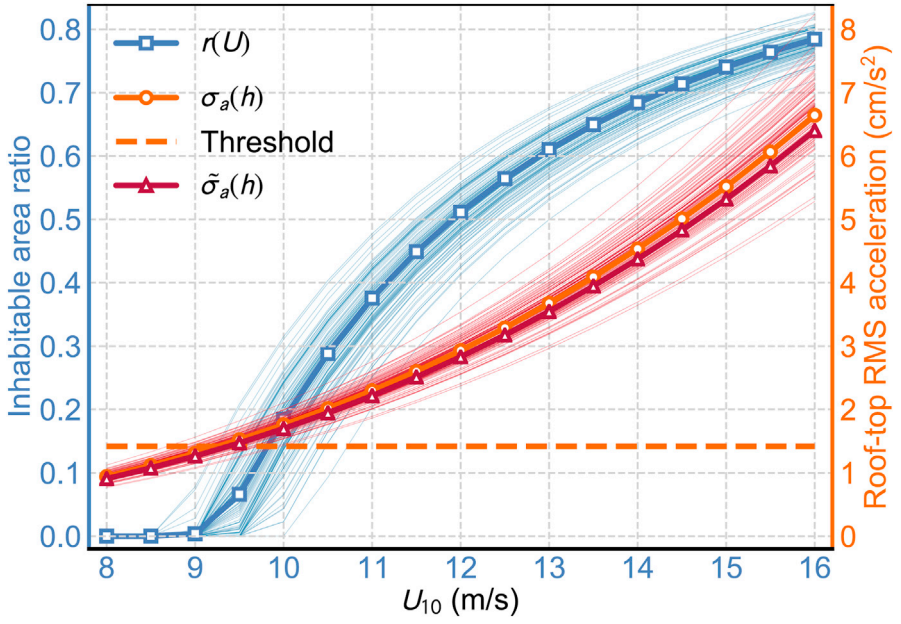

Fig. 2. 100 samples of CAARC building inhabitable area ratios and roof-top RMS accelerations at different wind speeds from Monte Carlo simulations (U_{10} is the mean wind speed at $z = 10$ m).

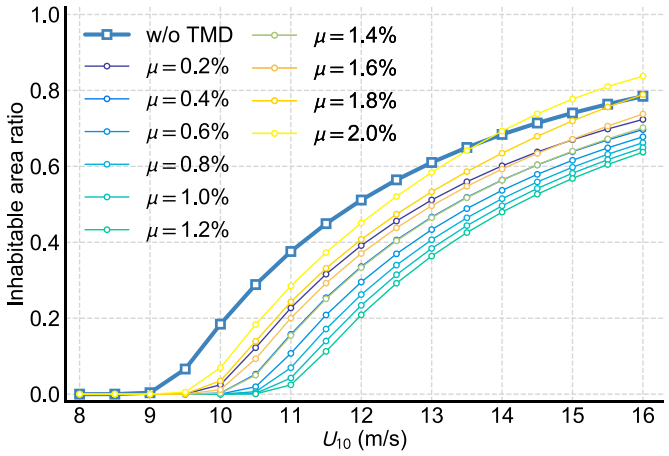

Fig. 3. CAARC building equipped with TMD - inhabitable area ratio at different wind speeds (U_{10} is the mean wind speed at $z = 10$ m).

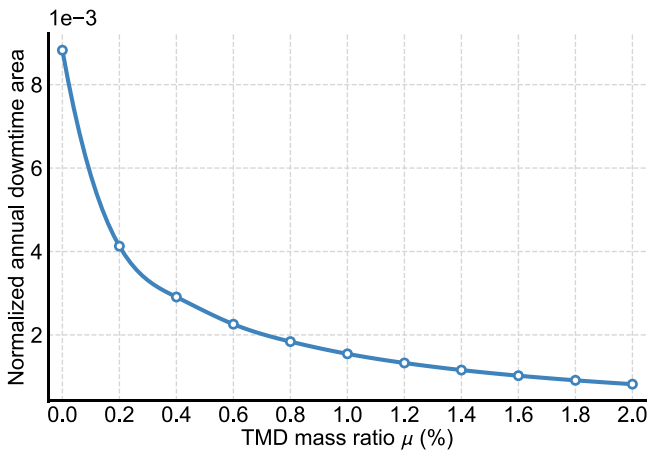

Fig. 6. Normalized annual inhabitable area ratio $\Gamma(\mu)$ for the full-scale CAARC building with and without TMD.

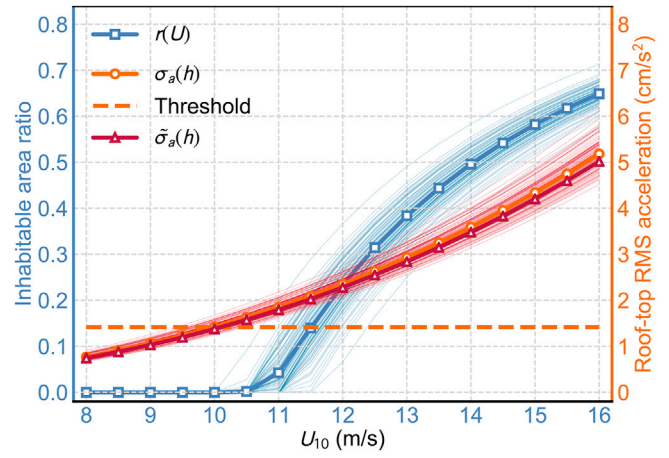

Fig. 4. 100 samples of CAARC building inhabitable area ratios and roof-top RMS accelerations equipped with TMD with $\mu = 0.2$ % at different wind speeds from Monte Carlo simulations (U_{10} is the mean wind speed at $z = 10$ m).

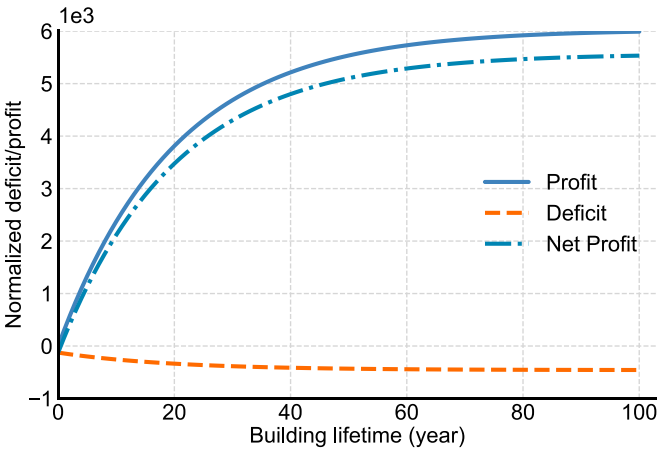

Fig. 7. The financial deficit and profit from TMD with $\mu = 0.2\%$ for the full-scale CAARC building.

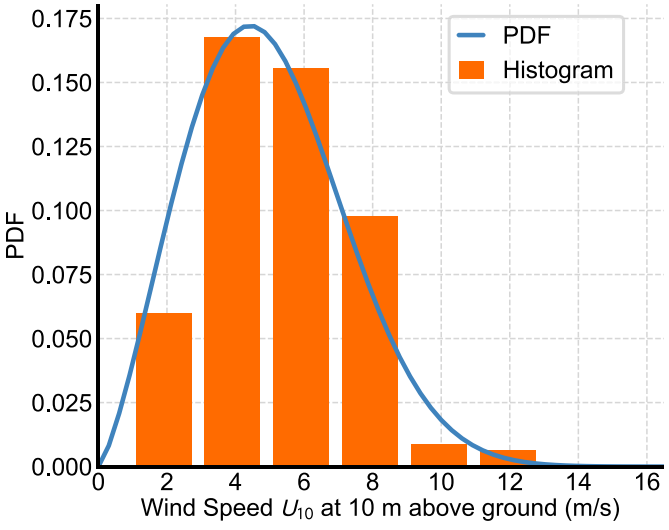

Fig. 5. Distribution of marginal parent mean wind speed U_{10} at the reference building site.

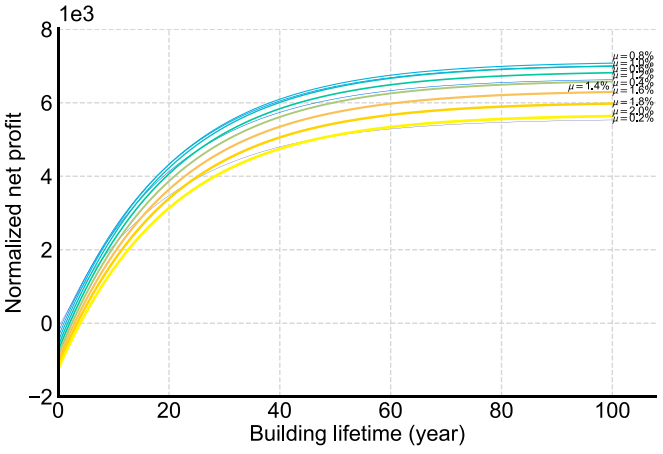

Fig. 8. Life-cycle financial profit from TMD with different mass ratio μ for the full-scale CAARC building.

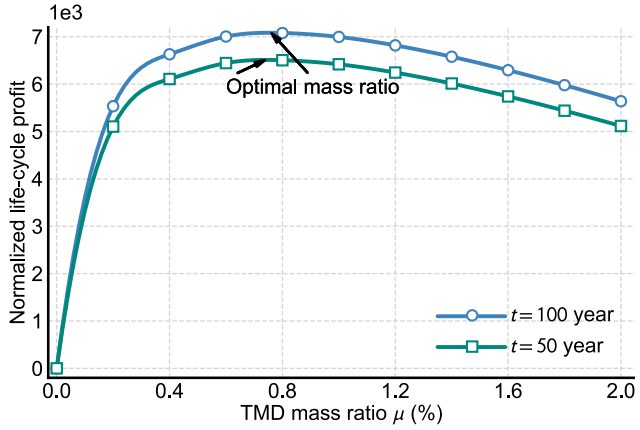

Fig. 9. Normalized annual inhabitable area ratio $\Gamma(\mu)$ for the full-scale CAARC building with and without TMD.

At last, the damper installation cost is assumed proportional to the damper mass:

$$c_i(\mu) = \Omega \times \mu \times m_{0,j} \tag{15}$$

where Ω is the mass to cost conversion factor, which is assumed as 0.003.

Initially, the mass ratio is set as 0.2%. The cost-benefit of TMD installation is closely examined. The profit part of Eq. (12): $(\Gamma_0 - \Gamma(\mu))A_f\frac{1-\exp(-\delta t)}{\delta}$ and the deficit part $A_d(\mu)\frac{1-\exp(-\delta t)}{\delta} + c_i(\mu)$ are respectively plotted as a dashed-dotted line and dashed line in Fig. 7. The overall net profit $c(t; 0.2\%)$, combining profit and deficit, is also calculated and plotted in Fig. 7.

Following the same procedure, the net profit of CAARC building with a variable mass ratio μ TMD is presented in Fig. 8. Results suggest that different mass ratios μ will induce different profit expectations. The profit comparison also depends on the structural lifetime. For the building with a short lifetime, a low-mass TMD is more suitable. For longer lifetimes, such as 50 or 100 years, $\mu = 0.8\%$ is the best value compared to other mass ratios.

Since cost analysis is initially performed considering discrete increments of mass ratio μ, spline interpolation is employed for optimization purposes and to compute the lifetime profit for the intermediate values between two consecutive discrete mass ratios (Fig. 9). Two typical lifetime values are analyzed: 50 and 100

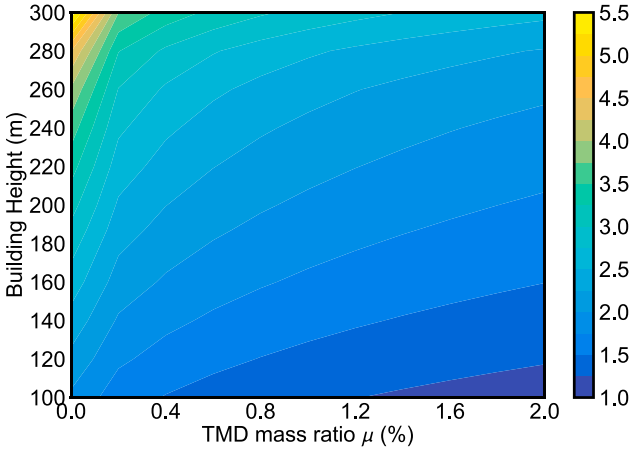

Fig. 10. Roof-top RMS acceleration of tall buildings with variable height h and different TMD mass ratios μ with reference wind speed at $z = 10$ m $U_{10} = 12$ m/s (units: cm s^{-2}).

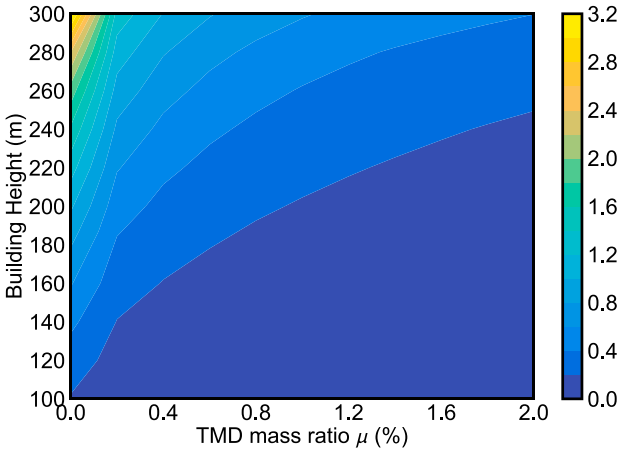

Fig. 11. Normalized annual inhabitable area ratio $\Gamma(\mu)$ for tall buildings with variable height h and different mass ratios μ (units: %).

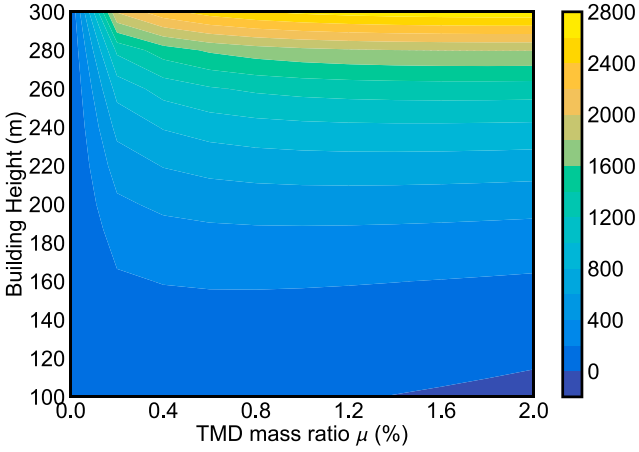

Fig. 12. Annual net profit associated with TMD installation as a function of TMD mass ratio μ in a tall building with variable height h.

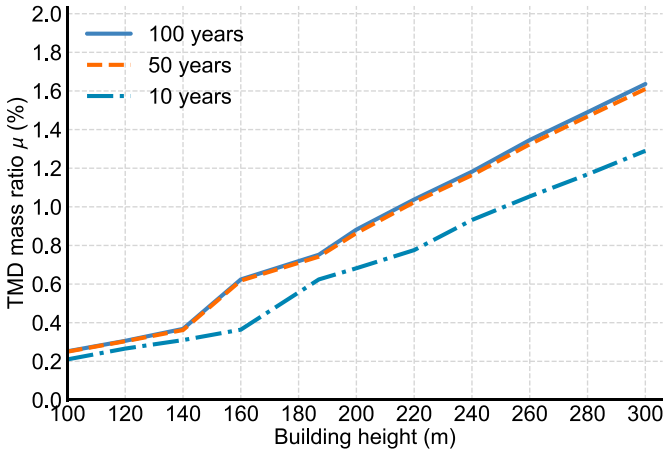

Fig. 13. Optimal TMD mass ratio as a function of building height and design lifetime.

years. In both cases, the optimal mass ratio is located between 0.7% and 0.8%. For the CAARC building with a 50-year lifetime, the optimal mass ratio is 0.73%, which is a little less than a 100-year lifetime.

4.4. Lifetime cost-benefit analysis for tall buildings with variable heights

After conducting the analysis for the CAARC benchmark building, equipped with TMD and different μ, the same procedure is extended to other tall buildings with variable height h.

The tall building height h is varied from 100 m to 300 m. The building floor plan is assumed the same as the CAARC building: $D = 45.7$ m and $B = 30.5$ m. The fundamental-mode structural frequency is assumed to be inversely proportional to the building height:

$$n_{0\{x,y\}}(h) \approx 0.2\frac{183}{h}\ [\text{Hz}] \tag{16}$$

in which h is the building height in meters, 183 m and 0.2 Hz are height and fundamental, lateral frequencies (x, y) of the CAARC building. The building mass is assumed the same one as the CAARC building (223224 kg/m).

All the wind field parameters and financial parameters are the same as the ones used in the previous section. The wind-induced acceleration of a tall building, equipped with TMD, can be calculated using the formulas listed in the previous section. For example, when the mean wind speed at $z = 10$ m U_{10} is 12 m/s, the roof-top acceleration for different building heights and TMD mass ratios is plotted in Fig. 10.

Subsequently, the building normalized annual inhabitable area ratio $\Gamma(\mu)$ is derived using Eqs. (7) and (8). The results in Fig. 11 suggest that, for a tall building without TMD, the annual inhabitable area drastically increases as the building height increases. On the other hand, the TMD is very effective for structural vibration reduction. For intermediate-height buildings, wind-induced vibration amplitudes are lower and the benefit of TMD installation is marginal.

Finally, the cost-benefit analysis associated with TMD installation can be assessed by Eq. (12), as illustrated in Fig. 12. The results clearly indicate that, for low-rise buildings, the TMD has a negative effect in terms of financial benefit, since the annual net profit is less than 0. For taller buildings, an optimal TMD mass ratio may be found, for which the annual net profit is maximized. Taking into account the TMD installation cost at the beginning of building lifetime, the optimal TMD mass ratio for buildings with variable height is plotted in Fig. 13. It is shown that, for a standard building design lifetime (either 50 years or 100 years), the optimal mass ratio is very close. However, for a shorter lifetime, typical of a temporary building, the optimal mass ratio is smaller since the initial installation cost has more impact on the overall financial return evaluation.

Appendix A. Brief description of the CAARC benchmark building

5. Conclusions

For tall buildings equipped with TMD systems under the effect of wind loads, the financial decision-making analysis tools are inadequate. Current methods exclusively calculate the building's maximum accelerations for selected wind speeds with short return periods. They cannot accurately evaluate the monetary impact associated with the installation of the TMD. This study examined a novel feasibility method to analytically calculate the profit and deficit of TMD as well as the effect of initial installation cost and variable TMD mass ratio. This framework consists of three modules:

1. Wind speed probability distribution at the building site;
2. Wind-induced structural vibration considering TMD installation;
3. Normalized annual inhabitable area and lifetime net profit of TMD.

The main findings of this paper are:

1. Numerical results suggest that, for middle-rise buildings ($100 < h < 120$ m), TMD installation cannot produce large financial benefit and sometimes introduces a deficit to building's overall income;
2. For high-rise buildings ($h > 120$ m), a TMD designed with an optimized mass ratio is beneficial;
3. However, a TMD with a large mass ratio must be avoided since it will reduce relevant profit. Optimized TMD mass ratio generally increases with building height.

Evaluation of the financial impact of TMD can be improved by considering wind directionality. This aspect may be examined in future studies.

CRediT authorship contribution statement

Wei Cui: Writing - original draft, Project administration, Conceptualization, Data curation. **Teng Ma:** Validation, Visualization. **Luca Caracoglia:** Supervision, Writing - review & editing.

Declaration of competing interest

The authors declare that they have no known competing financial interests or personal relationships that could have appeared to influence the work reported in this paper.

Acknowledgments

The authors gratefully acknowledge the support of National Natural Science Foundation of China (52008314) and Shanghai Pujiang Plan (No. 19PJ1409800). The third author also acknowledges the support of the National Science Foundation of the United States of America, Award CMMI-1852678. Any opinions, findings and conclusions or recommendations are those of the authors and do not necessarily reflect the views of the sponsors.

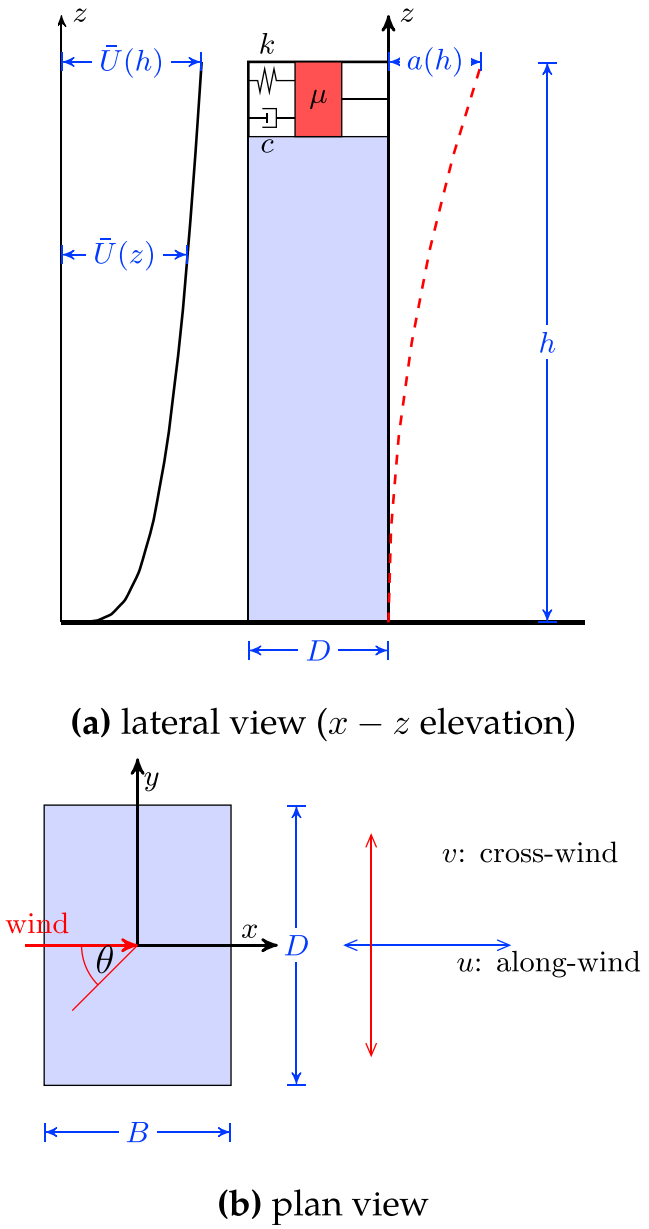

Fig. A.14. Schematic of the CAARC tall building equipped with TMD (Melbourne, 1980).

The CAARC benchmark building, which was proposed by the Commonwealth Advisory Aeronautical Research Council as a standard building structure for comparison of wind effects similarity among various wind tunnel laboratories (Melbourne, 1980), is used in this study to demonstrate the calculation procedure of the proposed analytical framework. The main procedures are briefly explained in this part.

This building has a uniform rectangular floor-plan. Its structural dynamic behavior can be modeled as a slender prismatic cantilever beam. The rectangular floor section is symmetrical about two principal, local axes of lateral bending (i.e., local Cartesian coordinate system denoted as x, y in Fig. A.14b). The mass is uniformly distributed along elevation z. Table A.2a and Table A.2b summarize the full-scale CAARC building structural properties and the corresponding wind field parameters that are employed in this study. Parameter definition can be found in Cui and Caracoglia (2020).

Table A.2
Benchmark building properties and corresponding wind field parameters (a) Structural parameters, (b) Wind field parameters

Quantity	Value
B [m]	30.5
D [m]	45.7
h [m]	183
$m(z)$ [kg/m]	223224
$\xi_{0,x} = \xi_{0,y} = \xi_0$	0.01

(*continued on next page*)

Table A.2 (*continued*)

Quantity	Value
$n_{0,x} = n_{0,y} = n_0$ [Hz]	0.2
$\varphi_x(z)$, $\varphi_y(z)$	$(z/h)^\gamma; \gamma = 1$
C_D	1.4
C_L	0
$\partial C_L / \partial\theta$	−3.5
ρ [kg/m3]	1.25
Roughness z_0 [m]	0.5
$U = U(h)$ [m/s]	0–50
$U(z)$ [m/s]	$U(z/h)^{0.28}$
u^* [m/s]	$U/2.5\ln(h/z_0)$
I_u	$0.53/\ln(h/z_0)$
C_{zu}	12
C_{zv}	$0.667C_{zu}$

Wind-induced vibrations can be computed using Eq. (1). Details may be found in Cui and Caracoglia (2018a). To verify model accuracy, the normalized, calculated mean and RMS values of structural vibration are compared against experimental values derived from Melbourne (1980); results are plotted in Fig. A.15.

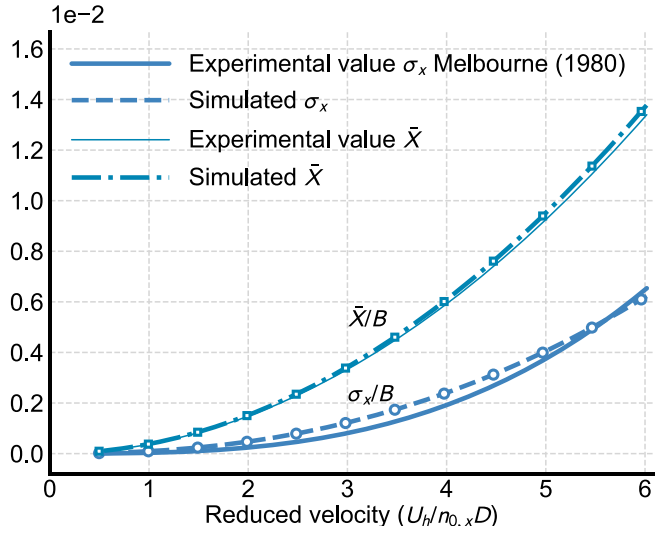

(a) Along-wind response

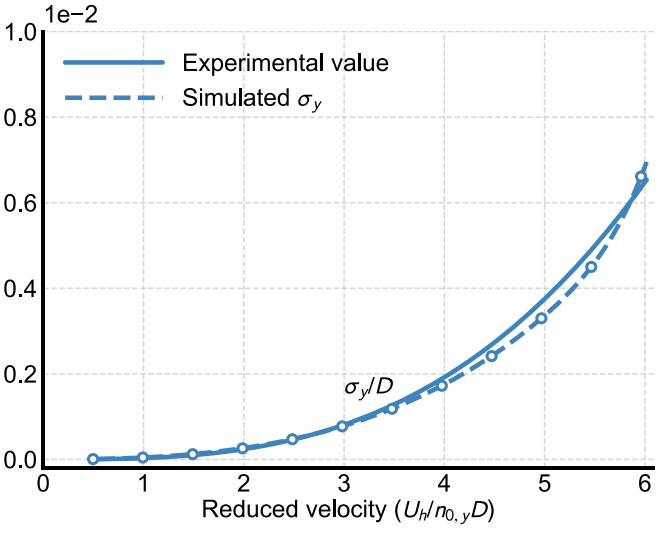

(b) Cross-wind response

Fig. A.15. Comparison between normalized, simulated response of the CAARC building and wind-tunnel experimental results derived from Melbourne (1980).

Good correspondence can be found; this result is the necessary evidence for the verification of the simulation method and parameters above.

Appendix BPreliminary, ''optimized'' TMD parameter search

For tall buildings equipped with TMD, the vibration can be calculated by Eq. (3). Without any loss of generality, given a specific TMD mass ratio μ, an approximate, suitably optimized configuration of TMD system can be derived under the assumption of white noise excitation. Although this hypothesis is, theoretically, only approximate for colored-noise turbulent load spectra, it is a common practice for tall building wind-induced analysis and vibration suppression (Xu et al., 1992). The frequency ratio γ and damping ratio ξ_j of optimal TMD can be approximately calculated, for example, using the "Sadek relationships'':

$$\gamma = \frac{1}{1+\mu}\left[1 - \xi_{0,j}\sqrt{\frac{\mu}{1+\mu}}\right] \tag{B.1}$$

$$\xi_j = \frac{\xi_{0,j}}{1+\mu} + \sqrt{\frac{\mu}{1+\mu}} \tag{B.2}$$

In Eqs. (B.1) and (B.2), the mass ratio is calculated with respect to the modal mass, in which the mode shape function should be normalized to have a unit participation factor. However, since one mode is exclusively considered in each primary direction, the mode shape function can be used without normalization. Furthermore, both the main wind force lateral force resisting systems and the TMD apparatus are usually excited at relative low amplitudes, associated with moderate wind load events; therefore, TMD malfunctioning (i.e. overshoot of maximum stroke) is not possible, and repair costs are not included in the cost-benefit analysis.

Table B.3 lists the optimal frequency and damping ratios calculated by Eqs. (B.1) and (B.2). The structural transfer function accounting for rooftop TMD, which is plotted in Fig. B.16, can be evaluated by Eq. (3) in the frequency domain. TMD with larger mass ratio can greatly reduce the amplification around the fundamental frequency. It should be noted that TMD manufacturers may not be able to tune the TMD to the exact optimal parameters, as shown in Table B.3; other factors, such as slight mis-tunning, minor changes of structural fundamental frequency and aging effect of TMD, will affect the TMD performance in the practical engineering application.

Table B.3
Optimal frequency and damping ratio of TMD with different mass ratio

μ	Γ	ξ_j	M	γ	ξ_j
0.002	0.998	0.055	0.012	0.987	0.119
0.004	0.995	0.073	0.014	0.985	0.127
0.006	0.993	0.087	0.016	0.983	0.135
0.008	0.991	0.099	0.018	0.981	0.143
0.010	0.989	0.109	0.020	0.979	0.150

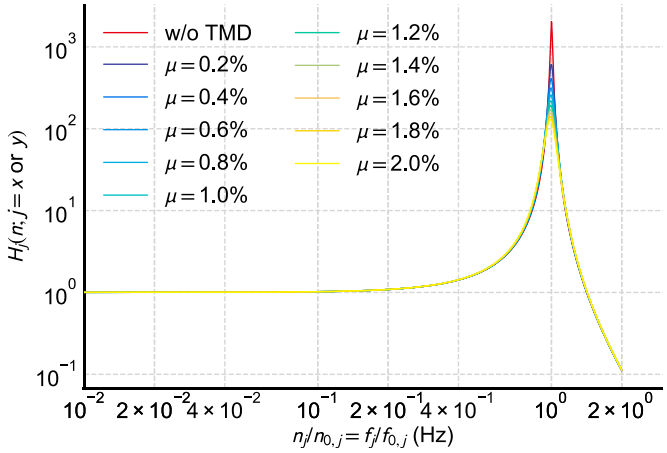

Fig. B.16. : Transfer function of a tall building with and without TMD.

References

ASCE, 2016. Minimum Design Loads for Building and Other Structures (ASCE 7-16).

Barbato, M., Palmeri, A., Petrini, F., 2014. Special issue on performance-based engineering. Eng. Struct. vol. 78, 1–2. Performance Based Engineering: Current Advances and Applications.

Bernardini, E., Spence, S., Gioffrè, M., Kareem, A., 2012. A reliability approach for the wind-induced response assessment of tall buildings using the high frequency force balance. In: The Seventh International Colloquium on Bluff Body Aerodynamics and Applications (BBAA7), pp. 825–834.

Bernardini, E., Spence, S.M., Kareem, A., 2013. A probabilistic approach for the full response estimation of tall buildings with 3d modes using the HFFB. Struct. Saf. 44, 91–101.

Carta, J.A., Ramírez, P., Bueno, C., 2008. A joint probability density function of wind speed and direction for wind energy analysis. Energy Convers. Manag. 49, 1309–1320.

Ciampoli, M., Petrini, F., Augusti, G., 2011. Performance-based wind engineering: towards a general procedure. Struct. Saf. 33, 367–378.

Cui, W., Caracoglia, L., 2018a. A fully-coupled generalized model for multi-directional wind loads on tall buildings: a development of the quasi-steady theory. J. Fluid Struct. 78, 52–68.

Cui, W., Caracoglia, L., 2018b. A unified framework for performance-based wind engineering of tall buildings in hurricane-prone regions based on lifetime intervention-cost estimation. Struct. Saf. 73, 75–86.

Cui, W., Caracoglia, L., 2020. Performance-based wind engineering of tall buildings examining life-cycle downtime and multisource wind damage. J. Struct. Eng. 146, 04019179.

Davenport, A.G., 1988. The response of supertall buildings to wind. In: Second Century of the Skyscraper. Springer, pp. 705–725.

Denoël, V., 2009. Estimation of modal correlation coefficients from background and resonant responses. Struct. Eng. Mech.: Int. J. 32, 725–740.

Elias, S., Matsagar, V., 2017. Research developments in vibration control of structures using passive tuned mass dampers. Annu. Rev. Contr. 44, 129–156.

Elias, S., Matsagar, V., 2018. Wind response control of tall buildings with a tuned mass damper. J. Build. Eng. 15, 51–60.

Elias, S., Matsagar, V., Datta, T., 2019a. Dynamic response control of a wind-excited tall building with distributed multiple tuned mass dampers. Int. J. Struct. Stabil. Dynam. 19, 1950059.

Elias, S., Matsagar, V., Datta, T.K., 2019b. Along-wind response control of chimneys with distributed multiple tuned mass dampers. Struct. Contr. Health Monit. 26, e2275.

Ellingwood, B., Rosowsky, D., Li, Y., Kim, J., 2004. Fragility assessment of light-frame wood construction subjected to wind and earthquake hazards. J. Struct. Eng. 130, 1921–1930.

Emanuel, K., Ravela, S., Vivant, E., Risi, C., 2006. A statistical deterministic approach to hurricane risk assessment. Bull. Am. Meteorol. Soc. 87, 299–314.

Giaralis, A., Petrini, F., 2017. Wind-induced vibration mitigation in tall buildings using the tuned mass-damper-inerter. J. Struct. Eng. 143, 04017127.

Grigoriu, M., 1984. Crossings of non-Gaussian translation processes. J. Eng. Mech. 110, 610–620.

Ierimonti, L., Caracoglia, L., Venanzi, I., 2016. Probability-based direct numerical estimation of wind-induced non-structural damage on tall buildings. In: Eighth International Colloquium on Bluff Body Aerodynamics (BBAA VIII). Northeastern University, Boston, Massachusetts, USA.

Ierimonti, L., Caracoglia, L., Venanzi, I., Materazzi, A.L., 2017. Investigation on life-cycle damage cost of wind-excited tall buildings considering directionality effects. J. Wind Eng. Ind. Aerod. 171, 207–218.

Ierimonti, L., Venanzi, I., Caracoglia, L., 2018. Life-cycle damage-based cost analysis of tall buildings equipped with tuned mass dampers. J. Wind Eng. Ind. Aerod. 176, 54–64.

Inokuma, A., 2002. Basic study of performance-based design in civil engineering. J. Prof. Issues Eng. Educ. Pract. 128, 30–35.

Irwin, P.A., 2006. Exposure categories and transitions for design wind loads. J. Struct. Eng. 132, 1755–1763.

Isyumov, N., 1993. Criteria for acceptable wind-induced motions of tall buildings. In: Proceedings of the International Conference on Tall Buildings. CTBUH, Rio de Janeiro.

Kwok, K., Samali, B., 1995. Performance of tuned mass dampers under wind loads. Eng. Struct. 17, 655–667.

Kwok, K.C., Hitchcock, P.A., Burton, M.D., 2009. Perception of vibration and occupant comfort in wind-excited tall buildings. J. Wind Eng. Ind. Aerod. vol. 97, 368–380, 12th International Conference on Wind Engineering.

Lawson, T., 1978. The wind content of the built environment. J. Wind Eng. Ind. Aerod. 3, 93–105.

Le, V., Caracoglia, L., 2018. Computationally efficient stochastic approach for the fragility analysis of vertical structures subjected to thunderstorm downburst winds. Eng. Struct. 165, 152–169.

Le, V., Caracoglia, L., 2020. Life-cycle cost analysis of a point-like structure subjected to tornadic wind loads. J. Struct. Eng. 146, 04019194.

van de Lindt, J., Dao, T., 2009. Performance-based wind engineering for wood-frame buildings. J. Struct. Eng. 135, 169–177.

Melbourne, W.H., 1980. Comparison of measurements on the CAARC standard tall building model in simulated model wind flows. J. Wind Eng. Ind. Aerod. 6, 73–88.

NOAA, 2015. National data Buoy center. http://www.ndbc.noaa.gov/. (Accessed 30 September 2015).

Petrini, F., Giaralis, A., Wang, Z., 2020. Optimal tuned mass-damper-inerter (tmdi) design in wind-excited tall buildings for occupants' comfort serviceability performance and energy harvesting. Eng. Struct. 204, 109904.

Pozos-Estrada, A., 2018. A simple procedure to evaluate the wind-induced acceleration in tall buildings: an application to Mexico. Wind Struct. 27, 337–345.

Pozos-Estrada, A., Gómez, R., 2019. Parametric study of the use and optimization of tuned mass dampers to control the wind-and seismic-induced responses of a slender monument. Struct. Des. Tall Special Build. 28, e1633.

Pozos-Estrada, A., Hong, H., Galsworthy, J., 2010. Serviceability design factors for wind-sensitive structures. Can. J. Civ. Eng. 37, 728–738.

Pozos-Estrada, A., Hong, H., Galsworthy, J., 2011. Reliability of structures with tuned mass dampers under wind-induced motion: a serviceability consideration. Wind Struct. 14, 113–131.

Pozzuoli, C., Bartoli, G., Peil, U., Clobes, M., 2013. Serviceability wind risk assessment of tall buildings including aeroelastic effects. J. Wind Eng. Ind. Aerod. 123, 325–338. Part B.

Rizzo, F., Caracoglia, L., Montelpare, S., 2018. Predicting the flutter speed of a pedestrian suspension bridge through examination of laboratory experimental errors. Eng. Struct. 172, 589–613.

SEAOC, 1995. Vision 2000: Performance Based Seismic Engineering of Buildings. Structural Engineers Association of California, Sacramento, California.

Seo, D.W., Caracoglia, L., 2012. Statistical buffeting response of flexible bridges influenced by errors in aeroelastic loading estimation. J. Wind Eng. Ind. Aerod. 104, 129–140.

Seo, D.W., Caracoglia, L., 2013. Estimating life-cycle monetary losses due to wind hazards: fragility analysis of long-span bridges. Eng. Struct. 56, 1593–1606.

Simiu, E., Yeo, D., 2019. Wind Effects on Structures: Modern Structural Design for Wind, 4 ed. Wiley–Blackwell, New Jersey, USA.

Spence, S.M., Kareem, A., 2014. Performance-based design and optimization of uncertain wind-excited dynamic building systems. Eng. Struct. 78, 133–144.

Vickery, P.J., Skerlj, P.F., Twisdale, L.A., 2000. Simulation of hurricane risk in the U.S. using empirical track model. J. Struct. Eng. 126, 1222–1237.

Wen, Y.K., Kang, Y.J., 2001. Minimum building lifecycle cost design criteria. I: Methodology. J. Struct. Eng. 127, 330–337.

Xu, Y., Kwok, K., Samali, B., 1992. Control of wind-induced tall building vibration by tuned mass dampers. J. Wind Eng. Ind. Aerod. 40, 1–32.

Yang, J.N., Agrawal, A.K., Samali, B., Wu, J.C., 2004. Benchmark problem for response control of wind-excited tall buildings. J. Eng. Mech. 130, 437–446.